RESEARCH ARTICLE

INTERNATIONAL RESEARCH JOURNAL OF MULTIDISCIPLINARY TECHNOVATION

Asian Research Association

DOI: 10.54392/irjmt2464

Comprehensive Theoretical Insights on Spectroscopic Characterization, Solvent Effect (Polar and Nonpolar) in Electronic behavior, Topological Insights, and Molecular Docking Prediction of Taurolidine

A. Mani [a], R. Elaiyaraja [a,*]

[a] PG and Research Department of Microbiology, Shanmuga Industries Arts and Science College, Tiruvannamalai -606603, Tamil Nadu, India

* Corresponding Author Email: r.elaiyaraja@yahoo.in

DOI: https://doi.org/10.54392/irjmt2464

Received: 30-08-2024; Revised: 29-10-2024; Accepted: 06-11-2024; Published: 11-11-2024

Abstract: In recent decades, sulfur-containing compounds have played a significant role in biological applications because of their unique biological and chemical characteristics. Taurolidine, a sulfur-containing derivative of the amino acid taurine, has been characterized theoretically utilizing Density Functional Theory (DFT) at the B3LYP approach along with a 6-311++G(d,p) basis set. The impact of solvents on electronic characteristics, Molecular electrostatic potential (MEP), and Fourier Molecular Orbital (FMO) in polar (water and ethanol) and nonpolar (toluene and chloroform) has been analyzed. The bond distances of S1-C16 and S1-C17 have been simulated at 1.817 Å and observed at 1.743 and 1.739 Å, respectively. These distances are increased compared to other bond distances due to the influence of sulfur atoms. The distinctive simulated vibrational wavenumbers of taurolidine revealed peaks for SO_2, CH_2, CN, and NH groups. The intramolecular interactions responsible for stabilizing the molecular structure of taurolidine have been addressed using NBO analysis shows significant stabilization energy from electron-donating lone pair oxygen O6 to antibonding S2-N10 with the stabilizing energy of 19.88 KJ/mol by the transition of LP(3)- σ*. The bonding characteristics and reactive sites (electron-rich and electron-poor) have been confirmed with Mulliken and MEP analysis. The carbons (C17 and C16) emphasize the increased negative potential due to the sulfonyl (SO_2) group in the ortho position. The topological insights, ELF and LOL, were spotted using Multiwfn software, highlighting the localized and delocalized electron regions within the crystal structure. In addition, molecular docking was performed to predict the antagonist activity of taurolidine against β-catenin protein, yielding a binding energy of -6.86 KJ/mol, which confirms its antiproliferative property.

Keywords: Taurolidine, DFT, Solvent effect, NBO, Molecular Docking

1. Introduction

Sulfur-containing compounds play a prominent role in medicinal chemistry and drug discovery due to their unique biological and chemical characteristics [1]. Sulfur-containing compounds with many pharmaceutical and biological applications can exist in various forms, such as sulfoxide, sulfonamide, sulfones, thioesters, and sulfamides [2]. Volatile sulfur compounds are found in small fractions in food, influencing desirable and undesirable odors [3, 4]. However, sulfur is the sixth most prevalent micromineral found in breast milk. In addition, sulfur-containing amino acids play a crucial role in stabilizing protein structures, metabolism, and detoxification [5, 6]. Taurolidine chemically (1,1-dioxoperhydro-1,2,4-thiabiazinan-4yl) methyl is a small dimeric compound with a molecular formula and weight of C7H16N4O4S2 and 284.4 g/mol a derivative of non-essential sulfur-containing amino acid taurine [7]. From the structural interpretation, taurolidine comprises two taurinamide rings linked together by methylene (CH_2) group. The taurinamide rings have sulfonyl (SO_2) groups in the ortho position concerning the N-H group. Taurolidine was chemically derived from benzyl (2-sulfamoylethyl) carbamate as a starting material by a two-step reaction process [8]. Taurolidine has anti-inflammatory, antiadherence, antiendotoxin, and antibacterial properties [9]. In addition, taurolidine prevents biofilm formation in catheters during peritoneal dialysis to prevent peritonitis [10]. Taurolidine exhibits antiviral activity against the influenza H5N1 virus by downregulating the NF-κB signaling pathway [11]. Taurolidine downregulates polypeptide cytokines activated by bacterial endotoxin in human peripheral

blood mononuclear cells at a concentration of 40-100 µg/mL [12].

Density Functional Theory (DFT) is a computational theoretical simulation approach that is more flexible, cost-effective, and reliable in predicting the molecular structures of natural and synthesized compounds [13, 14]. According to the existing literature, the theoretical and experimental spectroscopic approach to sulfur-containing drugs such as modafinil and topiramate have been reported [15, 16]. In addition, a complete set of simulated spectroscopic properties of sulfonamide drugs such as sulfadiazine, sulfamerazine, and sulfamethazine have been reported earlier using DFT with CAM-B3LYP, B3PW91, and BLYP level theories using 6-311++G(d,p) basis set [17]. Surprisingly, no extensive simulation or experimental spectroscopic approach to the molecular structure of taurolidine has yet to be reported. Bearing this reason in mind, our present study explores the structural, electronic, and spectroscopic characterization of taurolidine, which has been reported using the quantum chemical computational method.

2. Material and methods

2.1 Computational details

The level of theory integrated into quantum chemical computations plays a crucial role in determining the accuracy of the predictions. Complete theoretical simulations of taurolidine were carried out using the DFT/B3LYP/6-311++(d,p) basis set, implemented in the Gaussian 09W software package [18-21]. The electronic (UV-visible) and FMO characteristics of taurolidine were carried out with the support of Time Dependent-Density Functional Theory (TD-DFT) [22-25]. The Density of States (DOS) spectrum for taurolidine in solvents (polar and nonpolar) were calculated using the GaussSum program [26]. In addition, NBO, Mulliken charge distribution, and MEP were simulated with DFT/B3LYP using the same basis set to predict the intra and intermolecular hyperconjugations and reactive sites within the molecular structure of taurolidine. The Chemcraft program and GaussView 6 package were employed to represent outputs [27, 28] visually. The Topology analyses of taurolidine were simulated using Multiwfn software [29]. Moreover, the AutoDock4 tool was utilized for molecular docking prediction, offering a dependable platform to assess the interactions and developing essential insights into the potential biological characteristics of taurolidine [30]. The visual outputs of protein-ligand complex in 3D and 2D formats were analyzed with the aid of PyMOL visuvalizing tool and LigPlot+ programs [31, 32].

3. Results and discussions

3.1 Optimized geometry

The optimized taurolidine molecular structure was calculated using DFT/B3LYP with a 6-311++G(d,p) basis set, with atomic numbering displayed in Fig. 1. The findings of the structural parameters (bond angles and lengths) are illustrated in the Table. 1. The optimized structure of taurolidine has thirty-two different types of bond distances, such as four (S-O), two (S-C, C-C, and N-H), eight (N-C), and fourteen (C-H) bond distances. In the same way, taurolidine has fifty-six different types of band angles, such as two (O-S-O, N-C-C, S-C-C, and C-N-H), three (N-C-N), four (O-S-C and S-C-H), six (C-N-C), sixteen (N-C-H), seven (H-C-H), eight (C-C-H) angles, compared with crystal structure available in the literature [33].

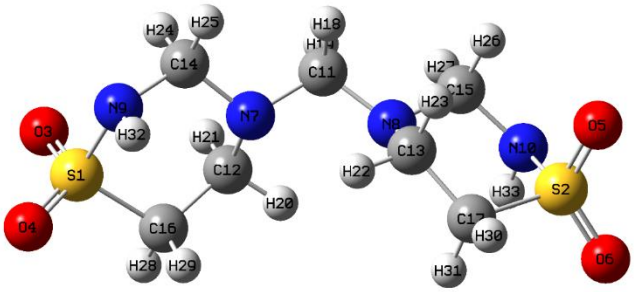

Figure 1. Optimized molecular structure of taurolidine

The molecular structure of taurolidine comprises two sulfonyl (SO_2) groups that give rise to four S-O bond distances simulated within 1.457-1.459 Å and observed at 1.422-1.436 Å. The bond angle of O3-S1-O4 and O5-S2-O6 were computed at 122.2 and observed at 119.4˚. The bond distances of S1-C16 and S1-C17 have been simulated at 1.817 Å and observed at 1.743 and 1.739 Å, respectively. Similarly, the bond angles of O-S-C, S-C-C, and S-C-H were computed between 107.5-110.0, 110.2, and 106.3-106.6˚ and observed at 105.8-111.6, 110.7-111.0, and 108.8-109.2˚, respectively. The bond distance of N9-H32 and N10-H33 in the ortho position of the sulfonyl (SO_2) groups have been calculated at 1.016 and observed at 0.959 Å. The bond angles of C-N-C, N-C-H, N-C-N, and N-C-C were simulated between 111.9-112.6, 111.0-112.5, 106.9-112.4, and 111.7˚ and observed at 111.4-114.6, 109.9-115.6, 106.9-109.5, 114.5-114.9˚, respectively. In addition, the bond angle of C-N-H was simulated at 113.2 and observed at 107.2-108.2˚. The optimized structure of taurolidine has four nitrogen atoms linked to methylene (CH_2) groups, giving rise to eight N-C bond distances calculated between 1.458-1.469 Å and observed at 1.433-1.500 Å. The bond lengths of C-H and C-C have been computed within 1.531 and 1.091-1.103 Å and observed at 1.508-1.529 and 0.959-0.960 Å, respectively.

Table 1. Experimental and theoretical geometrical parameters of taurolidine

Bond lengths (Å)	B3LYP	Experimental	Bond lengths (Å)	B3LYP	Experimental
S_1-O_3	1.459	1.423	C_{11}-H_{18}	1.103	0.959
S_1-O_4	1.457	-	C_{11}-H_{19}	1.103	0.960
S_1-C_{16}	1.817	1.743	C_{12}-C_{16}	1.531	1.529
S_2-O_5	1.459	1.436	C_{12}-H_{20}	1.091	0.959
S_2-O_6	1.457	1.422	C_{12}-H_{21}	1.102	0.960
S_2-C_{17}	1.817	1.739	C_{13}-C_{17}	1.531	1.508
N_7-C_{11}	1.458	1.448	C_{13}-H_{22}	1.091	0.960
N_7-C_{12}	1.469	1.447	C_{13}-H_{23}	1.102	0.959
N_7-C_{14}	1.467	1.451	C_{14}-H_{24}	1.099	0.960
N_8-C_{11}	1.458	1.463	C_{14}-H_{25}	1.091	-
N_8-C_{13}	1.469	1.458	C_{15}-H_{26}	1.099	0.959
N_8-C_{15}	1.467	1.433	C_{15}-H_{27}	1.091	0.960
N_9-C_{14}	1.462	1.500	C_{16}-H_{28}	1.091	0.960
N_9-H_{32}	1.016	0.959	C_{16}-H_{29}	1.091	0.960
N_{10}-C_{15}	1.462	1.479	C_{17}-H_{30}	1.091	0.960
N_{10}-H_{33}	1.016	0.959	C_{17}-H_{31}	1.091	0.960
Bond angles (◦)	**B3LYP**	**Experimental**	**Bond angles (◦)**	**B3LYP**	**Experimental**
O_3-S_1-O_4	122.2	-	C_{13}-N_8-C_{15}	111.9	110.4
O_3-S_1-C_{16}	107.5	110.7	N_8-C_{13}-C_{17}	111.7	114.5
O_4-S_1-C_{16}	110.0	-	N_8-C_{13}-H_{22}	107.8	108.2
S_1-C_{16}-C_{12}	110.2	110.7	N_8-C_{13}-H_{23}	111.3	108.0
S_1-C_{16}-H_{28}	106.6	109.1	N_8-C_{15}-N_{10}	112.5	115.6
S_1-C_{16}-H_{29}	106.3	109.2	N_8-C_{15}-H_{26}	112.4	108.2
O_5-S_2-O_6	122.2	119.4	N_8-C_{15}-H_{27}	109.0	107.4
O_5-S_2-C_{17}	107.5	105.8	C_{14}-N_9-H_{32}	113.2	108.2
O_6-S_2-C_{17}	110.0	111.6	N_9-C_{14}-H_{24}	106.9	108.8
S_2-C_{17}-C_{13}	110.2	111.0	N_9-C_{14}-H_{25}	107.7	-
S_2-C_{17}-H_{30}	106.6	108.8	C_{15}-N_{10}-H_{33}	113.2	107.2
S_2-C_{17}-H_{31}	106.3	109.2	N_{10}-C_{15}-H_{26}	106.9	109.0
C_{11}-N_7-C_{12}	112.4	114.6	N_{10}-C_{15}-H_{27}	107.7	106.9
C_{11}-N_7-C_{14}	112.6	114.1	H_{18}-C_{11}-H_{19}	107.1	109.5
N_7-C_{11}-N_8	111.0	109.9	C_{16}-C_{12}-H_{20}	108.6	108.8
N_7-C_{11}-H_{18}	107.4	109.2	C_{16}-C_{12}-H_{21}	109.3	107.4
N_7-C_{11}-H_{19}	112.0	109.2	C_{12}-C_{16}-H_{28}	111.6	108.6
C_{12}-N_7-C_{14}	111.9	111.4	C_{12}-C_{16}-H_{29}	112.0	109.6
N_7-C_{12}-C_{16}	111.7	114.9	H_{20}-C_{12}-H_{21}	107.9	109.4
N_7-C_{12}-H_{20}	107.8	107.7	C_{17}-C_{13}-H_{22}	108.6	108.3
N_7-C_{12}-H_{21}	111.3	108.2	C_{17}-C_{13}-H_{23}	109.3	108.1
N_7-C_{14}-N_9	112.5	114.9	C_{13}-C_{17}-H_{30}	111.6	108.8
N_7-C_{14}-H_{24}	112.4	108.3	C_{13}-C_{17}-H_{31}	112.0	109.3
N_7-C_{14}-H_{25}	109.0	-	H_{22}-C_{13}-H_{23}	107.9	109.4
C_{11}-N_8-C_{13}	112.4	113.5	H_{24}-C_{14}-H_{25}	108.2	-
C_{11}-N_8-C_{15}	112.6	113.7	H_{26}-C_{15}-H_{27}	108.2	109.4
N_8-C_{11}-H_{18}	112.0	109.3	H_{28}-C_{16}-H_{29}	109.9	109.4
N_8-C_{11}-H_{19}	107.4	109.5	H_{30}-C_{17}-H_{31}	109.9	109.4

*Taken from Ref [32]

On the other hand, the bond angles of C-C-H and H-C-H were computed within 108.6-112.0, and 107.9-109.9˚ and the corresponding numerical experimental values fell between 107.4-109.3 and

109.4-109.5˚, respectively. The linear coefficient (R2) values between computed and experimentallyobserved findings of bond angles and distances of taurolidine were found at 0.98607 and 0.98607, respectively. The correlation graph for structural parameters in Figure 2 confirms the excellent correlation between taurolidine's

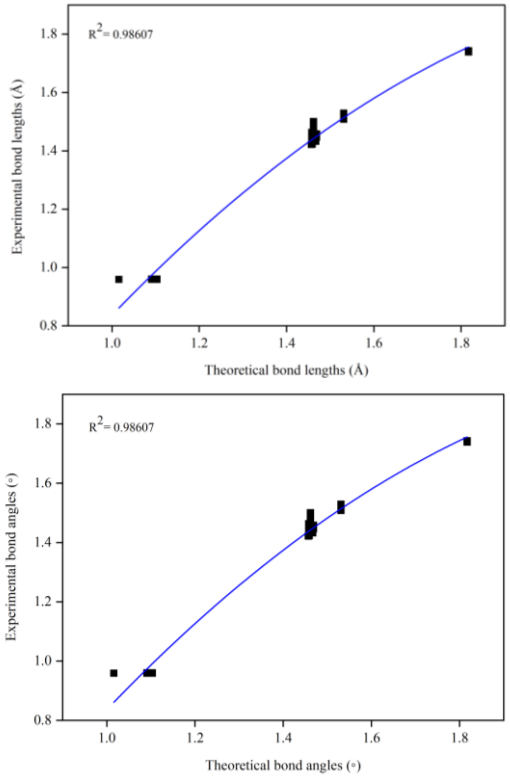

Figure 2. Correlation graph between experimental and theoretical bond lengths and bond angles of taurolidine computed and experimental findings.

3.2 Vibrational analysis

Taurolidine covers 33 atoms, and 150 electrons give 93 fundamental wavenumbers interpreting to 3N-6 with C1 point group symmetry. The simulated vibrational wavenumbers and the aggregating vibrational spectra are illustrated in Table 2 and presented in Figure 3. The potential energy distribution (PED) to confirm the potential vibrational modes exhibited by different functional groups. In addition, the calculated vibrational modes are scaled with a scaling factor of 0.96.

3.2.1 Stretching vibrations

Taurolidine has two sulfonyl (SO_2) groups in the ortho position concerning the N-H group, giving rise to SO_2 stretching modes. The SO_2 stretching modes for pyrazole borate derivatives were simulated at 1105 cm-1 and 1115 cm-1 for pyrazole pinacol esters [34]. The sulfonamide (SO_2) stretching mode was simulated in taurolidine at 1076 and 1072 cm-1 with a PED contribution of 70 and 69%, respectively. The anticipated N-H stretching modes in heterocyclic compounds fell between 3500-3320 cm-1 [35]. In taurolidine, the N-H group salvaged between sulfonyl (SO_2) and methylene (CH_2) groups gives rise to stretching modes at 3391 and 3389 cm-1 with a PED contribution of 100%. The titled compound comprises four nitrogen atoms linked with methylene groups, giving rise to C-N stretching modes. In nature, it is difficult to predict the C-N stretching wavenumbers due to the overlapping of multiple functional group bands that will appear in a similar region. The anticipated C-N stretching modes were felled between 1382-1266 cm-1 [36]. In taurolidine, the C-N modes were calculated at 1391, 1387, 1375, and 1352 cm-1. Typically, the methylene (CH_2) stretching wavenumbers are anticipated to occur between 3100-3000 cm-1 for asymmetric and 3000-2900 cm-1 for symmetric modes [37]. In taurolidine, the wavenumbers are simulated at 3011-2966 and 2915-2815 cm-1 for asymmetric and symmetric modes, respectively. The C-C stretching vibrations were felled within 1650-1200 cm-1 [**]. In taurolidine, the C-C stretching was simulated at 980, 972, and 959 cm-1 compared to the standard range; the wavenumbers have been simulated at the lower frequencies due to electron withdrawing sulfonyl (SO_2) and nitrogen groups influence the bond to stretch easily resulting in decreased wavenumbers.

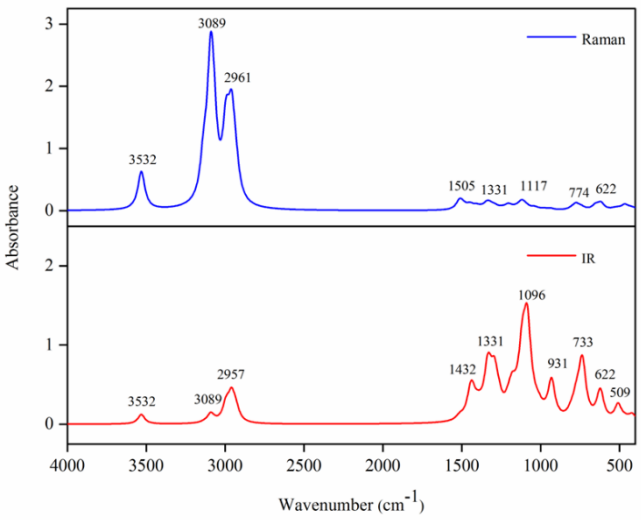

Figure 3. Simulated FT-IR and FT-Raman vibrational spectra of taurolidine

3.2.2 Bending vibrations

The CH_2 deformations in-plane (rocking and scissoring) and out-of-plane (twisting and wagging) manifest below 1500 cm-1 [38]. In taurolidine, the CH_2 deformations simulated below 1454 cm-1. In literature, the N-H deformation for 2TFBZ was simulated at 1199 and 1197 cm-1 and pioglitazone at 1199 cm-1 [39]. From these findings, the N-H deformation of taurolidine was simulated at 1387, 1375, 1336, 1292, and 1284 cm-1. In addition, the SO_2 scissoring modes of sulfonamide drugs at 569, 568, and 538 cm-1 for sulfadiazine, sulfamerazine, and sulfamethazine respectively [17]. In taurolidine, the scissoring modes were simulated at 513, 489, 414, and 301 cm-1 with a PED contribution of 40, 80, 18, and 10, respectively.

Table 2. Theoretical FT-IR and FT-Raman wave numbers of taurolidine

Modes	Theoretical wave numbers (cm^{-1})				Vibrational assignments (≥ 10% PED)
	Unscaled	Scaled	I_{IR}	SA_{Raman}	
1	3532	3391	22.43	60.46	υ NH (100)
2	3530	3389	21.91	61.72	υ NH (100)
3	3136	3011	1.51	53.93	$υ_{as}$ CH_2 (99)
4	3135	3010	1.93	62.53	$υ_{as}$ CH_2 (99)
5	3093.68	2970	7.78	198.39	$υ_{as}$ CH_2 (93)
6	3093.48	2969	4.16	14.16	$υ_{as}$ CH_2 (94)
7	3092	2968	13.11	89.49	$υ_{as}$ CH_2 (94)
8	3090	2966	15.10	87.59	$υ_{as}$ CH_2 (94)
9	3073.45	2951	1.77	76.11	$υ_s$ CH_2 (97)
10	3073.15	2950	2.39	106.6	$υ_s$ CH_2 (97)
11	2994	2874	64.61	179.85	$υ_s$ CH_2 (84)
12	2993	2873	11.58	34.03	$υ_s$ CH_2 (95)
13	2961	2843	61.02	66.53	$υ_{as}$ CH_2 (96)
14	2957	2839	9.86	165.78	$υ_s$ CH_2 (94)
15	2956	2838	45.57	13.32	$υ_s$ CH_2 (96)
16	2932	2815	51.50	72.82	$υ_s$ CH_2 (98)
17	1515	1454	9.54	19.85	β HCH (70)
18	1511	1451	7.32	1.37	β HCH (66)
19	1506	1446	0.56	8.72	β HCH (76)
20	1493	1433	2.85	2.10	β HCH (88)
21	1492	1432	0.70	6.09	β HCH (70)
22	1465	1406	2.43	2.12	τ HCNC (38)
23	1449	1391	4.29	3.78	υ CN (49)
24	1447	1389	0.19	1.17	β HCH (100)
25	1445	1387	87.63	8.27	β HNC (25), β HCH (34), υ CN (32)
26	1432	1375	74.92	0.18	β HNC (41), υ CN (46)
27	1408	1352	0.62	7.26	τ HCNS (10), τ HCNC (14), υ CN (18)
28	1399	1343	36.61	2.22	τ HCNC (41)
29	1392	1336	0.49	0.31	β HCN (11), τ HCNC (20), τ HCNS (11)
30	1377	1322	19.85	2.53	τ HCNS (14), τ HCNC (10)
31	1346	1292	12.71	9.22	β HCC (24), β HCN (10)
32	1338	1284	107.96	2.57	β HCN (13)
33	1337	1284	4.92	1.15	β HCC (32)
34	1331	1278	68.65	6.12	β HCN (10)
35	1323	1270	52.74	8.21	β HCN (17)
36	1293	1241	122.20	2.64	β HCN (23)
37	1292	1240	53.25	7.33	τ HCCN (10)
38	1265	1214	54.81	0.70	β HCC (10)
39	1245	1195	0.55	4.12	β HCC (32)
40	1215	1166	7.44	0.74	β HCC (21)
41	1206	1158	28.08	12.52	υ NC (21)
42	1185	1138	67.21	2.97	β HCC (16), τ HCCN (20)
43	1177	1130	47.21	0.77	β HCC (16)
44	1152	1106	36.08	4.43	υ NC (36)
45	1126	1081	1.66	2.62	υ NC (22)
46	1121	1076	0.65	14.76	υ SO_2 (70)
47	1117	1072	261.42	6.27	υ SO_2 (69)
48	1096	1052	25.06	8.17	υ NC (29)
49	1084	1041	369.01	2.30	υ NC (26)
50	1065	1022	28.28	0.04	υ NC (35)
51	1042	1000	19.11	0.45	τ HCNC (10)
52	1040	998	6.30	6.61	υ NC (32)
53	1021	980	0.63	1.21	υ CC (20)
54	1013	972	36.12	0.04	υ CC (32)

55	999	959	0.95	0.34	υ CC (42)
56	977	938	8.54	3.39	υ NC (38)
57	938	900	0.08	4.64	β CCN (24)
58	931	894	177.85	0.03	β CCN (22)
59	805	773	20.59	1.44	υ NC (33)
60	804	772	6.92	2.36	υ NC (29)
61	776	745	6.69	14.74	υ SN (27), τ HNCN (26)
62	774	743	69.08	3.72	υ SN (22), τ HNCN (25)
63	745	715	83.39	6.44	τ HNCN (42)
64	733	704	203.82	1.61	β NCN (28)
65	651.26	625	1.19	13.37	β NCN (27)
66	651.21	625	1.40	0.34	β NCN (14)
67	622	597	120.71	1.13	υ SN (21), τ HNCN (11)
68	617	592	19.14	19.75	υ SN (12). τ HNCN (10)
69	534	513	0.05	3.81	β OSO (40)
70	509	489	77.03	3.90	β OSO (80)
71	470	451	0.18	6.55	β NCN (11), τ OCOS (12)
72	469	450	3.34	1.37	β NCN (12), τ OCOS (11)
73	463	444	7.60	7.09	β CCN (12), τ OCOS (19)
74	462	156	1.09	1.15	β CCN (10), τ OCOS (21)
75	431	414	1.38	4.16	β OSO (18), τ OCOS (10)
76	421	404	30.04	1.73	τ OCOS (17)
77	406	390	0.01	2.51	τ CCCN (13)
78	388	372	4.59	1.42	β CNC (10), β OSN (12)
79	354	340	5.42	0.19	β CNC (34)
80	344	330	1.66	0.53	τ OCNS (26)
81	314	301	14.90	0.28	β OSO (10)
82	311	299	1.63	2.04	β CCN (10), β OSN (15), τ OCOS (10)
83	287	276	2.86	0.08	β OSN (11), τ OCNS (21)
84	234	225	0.58	0.66	τ OCNS (22)
85	224	215	4.10	0.03	β OSN (14)
86	222	213	0.35	3.84	β SNC (12), β OSN (12)
87	193	185	1.85	1.17	τ NCNC (10), τ SNCN (15)
88	188	180	4.35	0.08	τ CCNC (14)
89	103	99	1.87	0.60	β NCN (19), β SNC (20), τ CNCN (12)
90	99	95	3.25	0.17	τ NCNC (10), τ CNCN (12)
91	47	45	0.19	0.10	τ NCNC (32), τ CNCN (41)
92	37	36	6.95	0.29	τ NCNC (19), τ CNCN (29)
93	35	37	7.85	0.08	β NCN (17), β CNC (14), τ NCNC (33)

υ - stretching, υ_s - symmetric stretching, υ_{as} - asymmetric stretching, τ- torsion, ω- wagging, χ- scissoring, β- deformation. Theoretical wavenumber scaling factor: 0.96 for all vibrations.

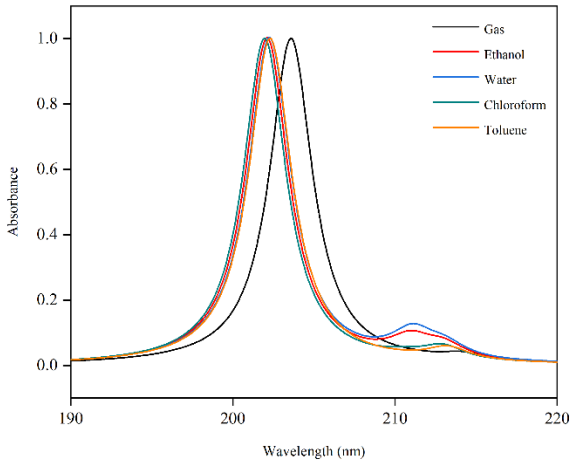

Figure 4. Simulated electronic spectra of taurolidine in gas, polar and nonpolar solvents

	Gas	Ethanol	Water
HOMO	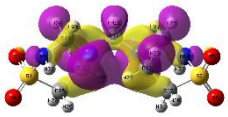	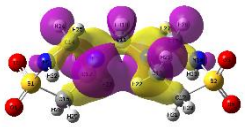	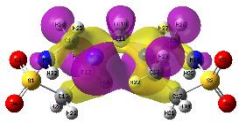
HOMO – LUMO (Eg)	Eg = 6.4667 eV	Eg = 6.5046 eV	Eg = 6.4973 eV
LUMO	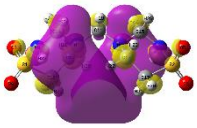	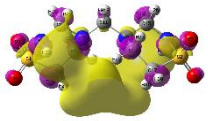	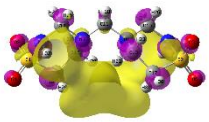

Figure 5(a). HOMO-LUMO energy gap of taurolidine in the gas phase and polar solvents

	Chloroform	Toluene
HOMO	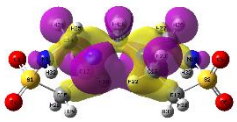	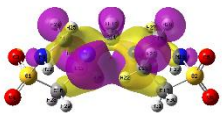
HOMO – LUMO (Eg)	Eg = 6.5286 eV	Eg = 6.8175eV
LUMO	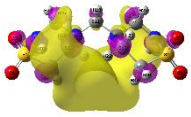	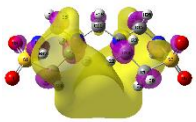

Figure 5(b). HOMO-LUMO energy gap of taurolidine in nonpolar solvents

3.3 Electronic properties

Taurolidine, a compound derived from the amino acid taurine, was selected based on the solubility characteristics of taurine. Taurine is known to be partially soluble in organic solvents and poorly soluble in water, influencing the choice of taurolidine solvents [40]. The computed electronic and Frontier Molecular Orbital (FMO) characteristics of taurolidine assess the stability and chemical reactivity of the molecular structure. The

simulation was made with different phases, such as gas, polar (water and ethanol), and nonpolar (toluene and chloroform) solvents. The computed electronic spectra and FMO (HOMO and LUMO) graphs of taurolidine are visualized in Figures 4 and 5 and the corresponding wavelengths, major and minor contributions, and FMO findings are tabulated in Tables 3 and 4. The compound with an increased HOMO-LUMO energy gap is more stable and has decreased chemical reactivity due to more energy required to promote the electrons from H→L transitions. Conversely, a reduced HOMO-LUMO energy gap indicates less stability and more reactivity due to reduced energy required for electrons from H→L transitions. In taurolidine, a strong peak was observed at 203 (gas), 202 (ethanol and water), and 201 (chloroform and toluene) by H→L transitions. The blue and aureate colors in the HOMO-LUMO map represent the occupied and unoccupied orbitals, respectively. In taurolidine, the simulated energy gap was felled at 6.4667 eV (gas), 6.5286 eV (chloroform), 6.8175 eV (toluene), 6.5046 eV (ethanol), and 6.4973 eV (water). Compared with polar solvents, nonpolar solvents have increased energy gaps and confirm their stability and reactivity in polar solvents. The energy gap of nonpolar solvent toluene has increased compared to other solvents, confirming the compound's increased stability and decreased chemical reactivity. The DOS spectrum of taurolidine in gas, polar, and nonpolar solvents is demonstrated in Figure 6.

3.4 NBO

In computational chemistry, NBO analysis is used to examine the molecular structure of compounds by understanding the bonding interaction and distribution of electrons [41]. In NBO, the bonding orbitals (BD) donor and antibonding orbital (BD*) acceptor interactions emphasize the stabilizing energies. The highest and lowest stabilizing energy corresponds to the molecular system's strongest donor-acceptor and weakest donor-acceptor interactions. In taurolidine, the NBO characteristics have been simulated using the DFT/B3LYP method with a 6-311++G (d,p) basis set; the numerical values are tabulated in Table 5. In taurolidine, the stabilization of interaction between electron-donating lone pair oxygen O6 to antibonding S2-N10 with the stabilizing energy of 19.88 KJ/mol by the transition of LP(3)- σ* contributes the maximum stabilization. The second major stabilizing energy from the lone pair oxygen O3 and O6 to antibonding S1-C16 and S2-C17 with the stabilizing energy of 18.48 KJ/mol by the transition of LP(2)- σ*. In addition, LP(2)- σ* transitions were also simulated between electron-donating lone pair oxygens O3, O4, O5 and O6 to anti-bonding S1-C16, S1-O4, S1-N9, S1-O3, S1-N5, S3-C17, S2-O6, S2-N10, and S2-O5 by LP(2)- σ* and LP(3)- σ* transitions.

3.5 Mulliken charge distribution

In computational chemistry, Mulliken charge distribution provides better insight into electron density distribution within the molecular structure, allowing for the prediction of intermolecular interactions, reactivity, and chemical properties [42]. Figure S1 (Supplementary material) shows the Mulliken distribution of charges in taurolidine, and the agreeing numerical values are tabulated in Table 6. In taurolidine, the carbon atoms C17 (-0.78141e) and C16 (-0.78142e) have increased negative potential as a result of the sulfonyl (SO_2) group in the ortho positions. The nitrogen atoms N9 (-0.28325e) and N10 (-0.28323e) have net negative potential linked with the sulfonyl (SO_2) group. Whereas the nitrogens N7 (0.235882e) and N8 (0.235866e) salvaged between the methylene (CH_2) groups have net positive potential due to reduced density of electrons around the nitrogens by the influence of methylene (CH_2) groups. As expected, the oxygen (O3-O6) and hydrogen (H18-H33) atoms have net negative and positive potentials. The sulfur atoms S1 (0.43790e) and S2 (0.437884e) linked with oxygen atoms attract the electrons towards themselves, making them an increased positive potential. In addition, the outputs were closely confirmed by MEP analysis.

3.6 MEP analysis

MEP analysis predicts the positive (electron-poor) and negative (electron-rich) regions in theoretical chemistry by generating the color map. The color map comprises red (electron-rich) and blue (electron-poor), which correspond to regions that donate and accept electrons during a chemical reaction. The MEP offers better insight into noncovalent interactions such as Van der Walls, hydrogen bonding, and electrostatic attraction and how they interact with other compounds. Fig. S2 (Supplementary material) illustrates the MEP color map of taurolidine in polar (water and ethanol) and nonpolar (chloroform and toluene) solvents. The electrostatic potential range of taurolidine was simulated between -5.865 x 10-2 to 5.865 x 10-2 e.s.u. (gas), -7.006 x 10-2 to 7.006 x 10-2 e.s.u. (ethanol), -7.077 x 10-2 to 7.077 x 10-2 e.s.u. (water), and -6.647 x 10-2 to 6.647 x 10-2 e.s.u. (chloroform and toluene). In taurolidine, the red region (electron-rich) masks over the oxygen atoms (O3, O4, O5, and O6) in the sulfonyl (SO_2) group site for nucleophilic reactive species. The blue (electron-poor) region covers the hydrogen atoms in the methylene (CH_2) groups, affirming the site for electrophilic reactive species. Solvents have increased electrostatic potential range in polar (water and ethanol) compared to nonpolar (toluene and chloroform) due to solvent-solute interactions. The negative potential around the oxygen atoms (O3, O4, O5, and O6) creates hydrogen bonding with positively charged hydrogen atoms in the enzymes or proteins.

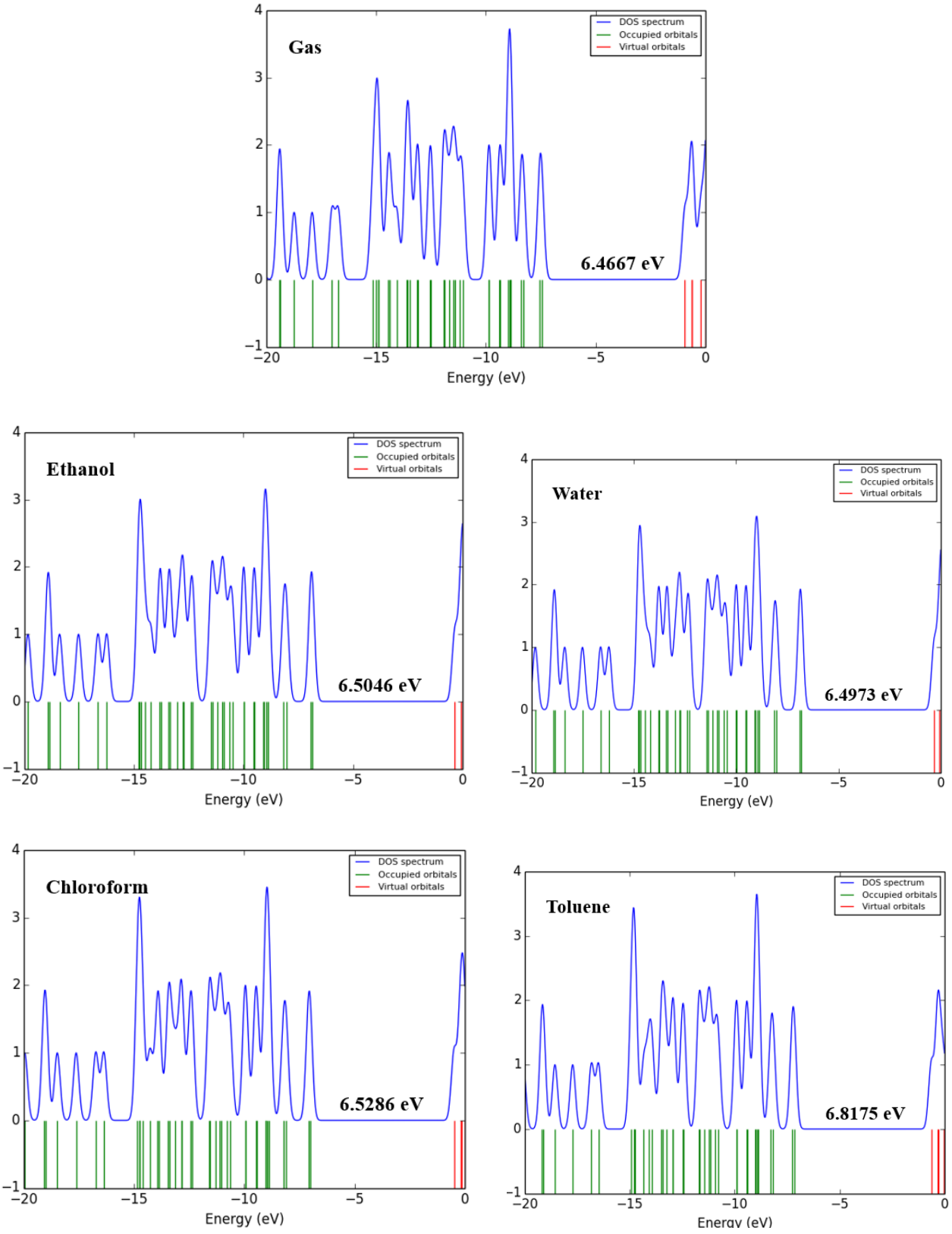

Figure 6. Simulated DOS spectrum of taurolidine in the gas phase, polar and nonpolar solvents

Table 3a. Calculated wavelengths (λ), excitation energies (E), and oscillator strengths (f) of taurolidine in gas phase and polar solvents

TDDFT /B3LYP/ 6-311++G(d,p)					
Gas	**λ (nm)**	**E (eV)**	**F**	**Major contributions**	**Minor contributions**
	214	5.79	0.0009	H→L (96%)	H-1→L+1 (2%)
	211	5.87	0.0001	H-1→L+1 (92%)	H→L+1 (6%)
	203	6.09	0.0456	H→L+2 (98%)	-
Ethanol	213	5.82	0.0021	H→L (94%)	H-1→L+1 (3%)
	210	5.87	0.0031	H-1→L (90%)	H→L+1 (7%)
	202	6.13	0.0517	H→L+1 (74%), H→L+3 (15%)	H-1→L (5%), H→L+2 (3%)
Water	213	5.81	0.0019	H→L (94%)	H-1→L+1 (3%)
	211	5.87	0.0039	H-1→L (90%)	H→L+1 (3%)
	202	6.12	0.0482	H→L+1 (73%), H→L+3 (16%)	H-1→L (6%), H-1→L+2 (3%)

Table 3b. Calculated wavelengths (λ), excitation energies (E), and oscillator strengths (f) of taurolidine in nonpolar solvents

TDDFT /B3LYP/ 6-311++G(d,p)					
Chloroform	**λ (nm)**	**E (eV)**	**F**	**Major contributions**	**Minor contributions**
	212	5.82	0.0026	H→L (95%)	H-1→L+1 (3%)
	210	5.88	0.0007	H-1→L (92%)	H→L+1 (6%)
	201	6.13	0.0622	H→L+1 (85%)	H-1→L (4%), H-1→L+2 (4%), H→L+3 (5%)
Toluene	213	5.81	0.0026	H→L (95%)	H-1→L+1 (2%)
	210	5.88	0.0001	H-1→L (92%)	H→L+1 (5%)
	201	6.12	0.0667	H→L (88%)	H-1→L (4%), H-1→L+2 (4%)

Table 4. The FMO energies and energy gap of taurolidine in gas phase, polar and nonpolar solvents

B3LYP/6-311G++ (d, p)	Formula	Gas	Chloroform	Ethanol	Toluene	Water
E_{HOMO} (eV)	-	-7.4605	-7.0145	-6.8537	-7.1666	-6.8235
E_{LUMO} (eV)	-	-0.9938	-0.4859	-0.3491	-0.6315	-0.3262
$E_{HOMO-LUMO}$ gap(eV)	-	6.4667	6.5286	6.5046	6.8175	6.4973
Ionization potential (I)	$-E_{HOMO}$	7.4605	7.0145	6.8537	7.1666	6.8235
Electron affinity (A)	$-E_{LUMO}$	0.9938	0.4859	0.3491	0.6315	0.3262
Electronegativity (χ)	(I+A)/2	4.2271	3.7502	3.6014	3.8990	3.5748
Chemical potential (μ)	-χ	-4.2271	-3.7502	-3.6014	-3.8990	-3.5748
Chemical hardness (η)	I-A	6.4667	6.5286	6.5046	6.8175	6.4973
Chemical softness (s)	1/2η	0.0773	0.0765	0.0768	0.0733	0.0769
Global Electrophilicity (ω)	$\mu^2/2\eta$	1.3851	1.0771	0.9969	1.1149	0.9834
Maximum electron charge (ΔNmax)	−(μ/η)	0.6536	0.5744	0.5536	0.5719	0.5501

3.7 Topological analysis

3.7.1 ELF and LOL

The ELF and LOL quantify the probability of electrons localized in specific regions. In addition, the ELF and LOL analyze the behavior of electrons, charge distribution, and density of electrons to get a better insight into atoms' molecular bonding and electronic behavior. In ELF, The high and low values signify localized electrons (red) and delocalized electrons (blue) in the molecular structure. In LOL, the yellow regions encircled with blue and the white region encircled with red represent the bonding interaction within the core atoms and valence cell, respectively [43]. The 3D plots of ELF and LOL illustrate the orbital distributions, forecasting better insight into taurolidine's crystal structure. The maps simulated within the range of 0 to 1 specify the delocalized and localized orbitals in the crystal structure. In the orbital graph, the values below 0.5 represent the delocalized regions, and values above 0.5 represent localized regions. The calculated ELF and LOL color-filled, contour, and projection maps for taurolidine have been illustrated in Figs. 7 and 8. In taurolidine, the hydrogens H24 (salvaged between nitrogen atoms) and H31 (linked with the sulfonyl group) are masked with red regions. In nature, a hydrogen atom comprises single electrons that form bonds with neighboring atoms by sharing. The red regions indicate localized electron density around the hydrogen atoms, likely due to the electronegative oxygen atoms forming polar bonds, which pull electron density towards the hydrogen atoms due to electrostatic effects. In addition, the blue rings cover the carbon C11, nitrogen N7, and sulfur S2 atoms, signifying the delocalized electron regions due to conjugated system electrons are shared and spread out in the aromatic system. In LOL, the white region is circled red, highlighting concentrated electrons around the atoms, and blue circles signify the delocalized electron regions. In taurolidine, the hydrogen atoms H24 and H31 are encircled with red color, and carbon C11, nitrogen N7, and sulfur S2 atoms are masked with blue rings, confirming localized and delocalized electron regions, respectively.

3.8 ADME prediction

ADME is a rapid screening method used in drug discovery to forecast the molecular properties of drugs (phytomedicines and synthetic compounds). According to Lipinski's criteria, a compound considered a drug has no more than one violation of the Lipinski rule of five. The molecular characteristics of taurolidine are tabulated in the Table. S1 (Supplementary material) and the consistent boiled egg and radar graph were illustrated in Fig. S3 (Supplementary material). From the findings, taurolidine comprises a molecular weight of 284.36 g/mol, with eight and two hydrogen bond donors and acceptors, respectively. According to Lipinski, the compound's molecular weight must be below 500 g/mol with less than five hydrogen bond donors and acceptors. From this observation, taurolidine confirms its potential bioactivity. In addition, the TPSA and lipophilicity values must be less than 140 Å2 and five, respectively. In contrast, taurolidine's TPSA and lipophilicity findings were simulated at 115.58 Å2 and -1.55, respectively. The pictorial boiled egg graph confirms that taurolidine has increased Gastrointestinal region (GI) absorption and Blood-brain barrier (BBB) penetration.

The bioavailability radar for taurolidine falls within the pink region, indicating that it possesses favorable properties for optimal bioavailability, which suggests a good balance of pharmacokinetic characteristics essential for effective therapeutic use. The Quantitative Estimate of Drug-likeness (QED) is a numerical value encompassing various physicochemical and structural properties. QED values range from 0 to 1, where a QED value of 1 indicates favorable drug-likeness properties, while 0 signifies poor drug-likeness. The QED score for taurolidine, simulated at 0.574 using ADMET Lab 2.0, suggests that the compound possesses moderate drug-likeness properties. These findings will help researchers conduct in vivo and in vitro drug discovery processes.

3.9 Molecular docking

Molecular docking is a simulation method used in drug designing and structural biology to forecast the orientation of a macromolecule (Protein) with a small molecule (ligand) [44, 45]. The molecular structure of the Protein (macromolecule) was extracted from the Protein Data Bank (PDB) with a resolution of 2.76 Å and kept in PDB format. The taurolidine (ligand) crystal structure was extracted from PubChem in SDF format, optimized using the GaussView 6 program without geometrical restriction, and saved in PDB format. The active site binding domain for the amino acid is enclosed within a grid box measuring 126×106×104 Å (X×Y×Z) for beta-catenin. The molecular docking simulation was performed between a ligand (taurolidine) and a macromolecule (3TX7), resulting in nine conformations. Among these, the conformation with the lowest docking energy was identified as the best. From the findings, taurolidine shows a binding affinity of -6.86 KJ/mol, characterized by hydrogen bonding and hydrophobic interactions. The ligand (taurolidine) exhibits two hydrogen bonds with the amino acids glutamic acid 505 and lysine 437 with a bond distance of 2.86 and 3.09 Å, respectively. In addition, taurolidine makes hydrophobic interactions with the amino acids histidine 430, glutamic acid 433, arginine 505, leucine 434, isoleucine 509, and alanine 508. The 3D and 2D interaction map of ligand and protein was illustrated in Figure 9 and presented in Table 7. β-catenin is a regulatory protein that activates genes responsible for cell proliferation, survival, and differentiation within the Wnt signaling pathway. Mutations in beta-catenin can contribute to

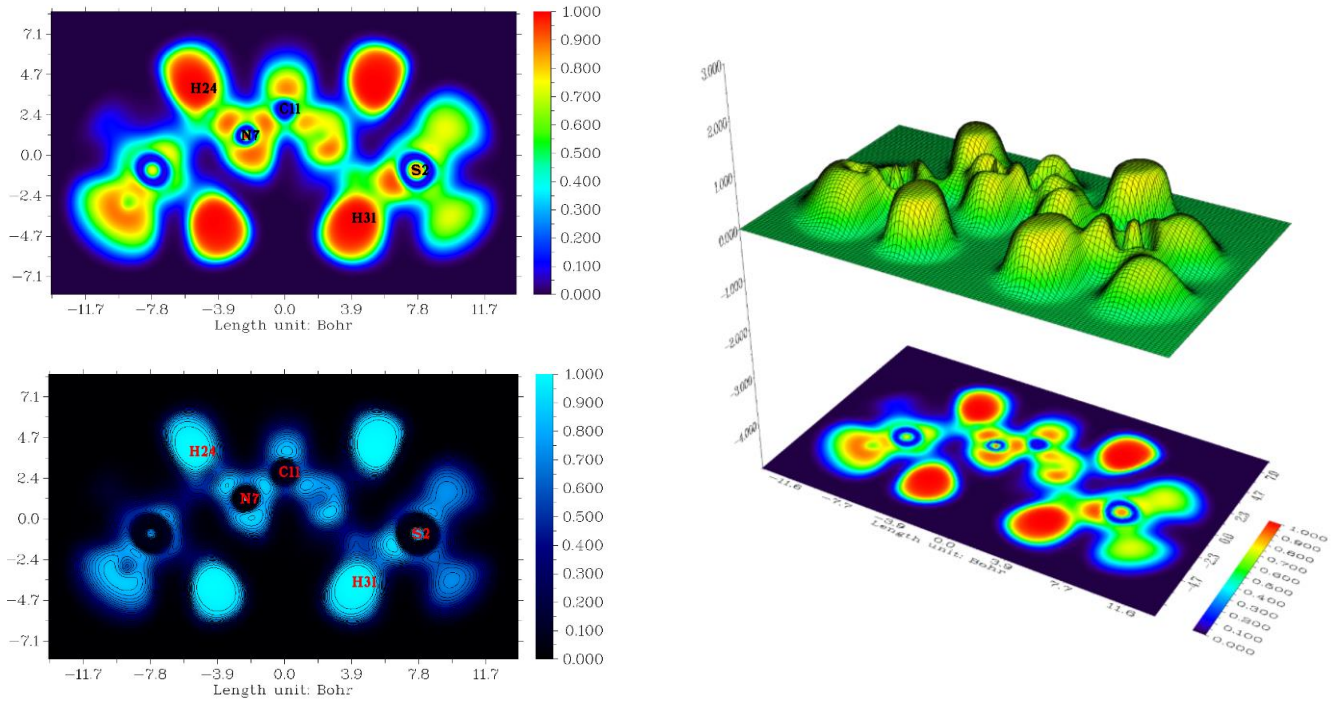

Figure 7. ELF Projection and Contour map of taurolidine

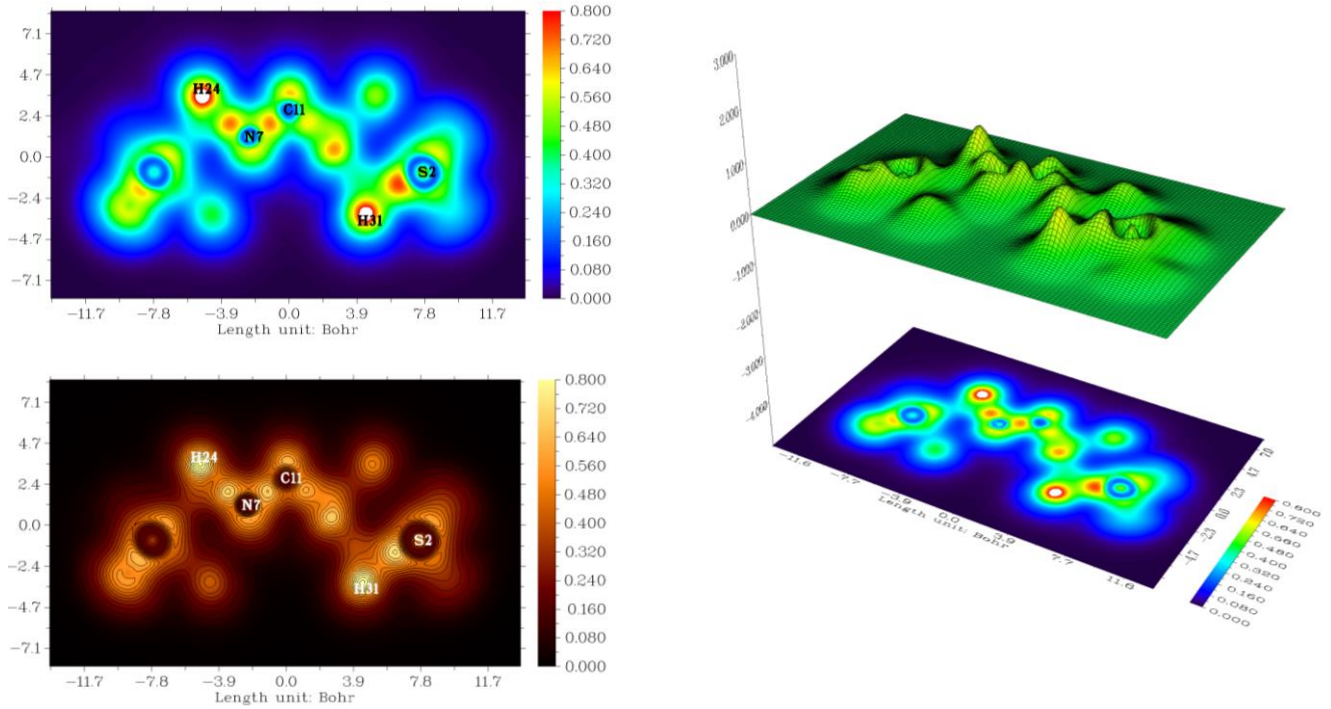

Figure 8. LOL Projection and Contour map of taurolidine

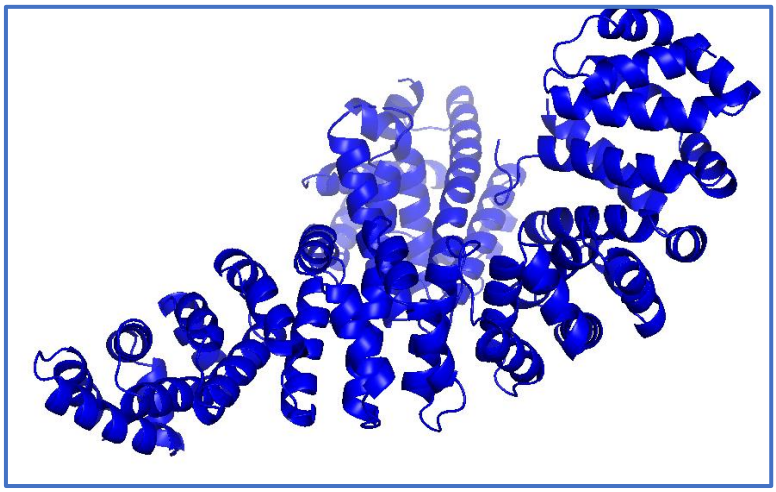

Figure 9a. Native structure of protein

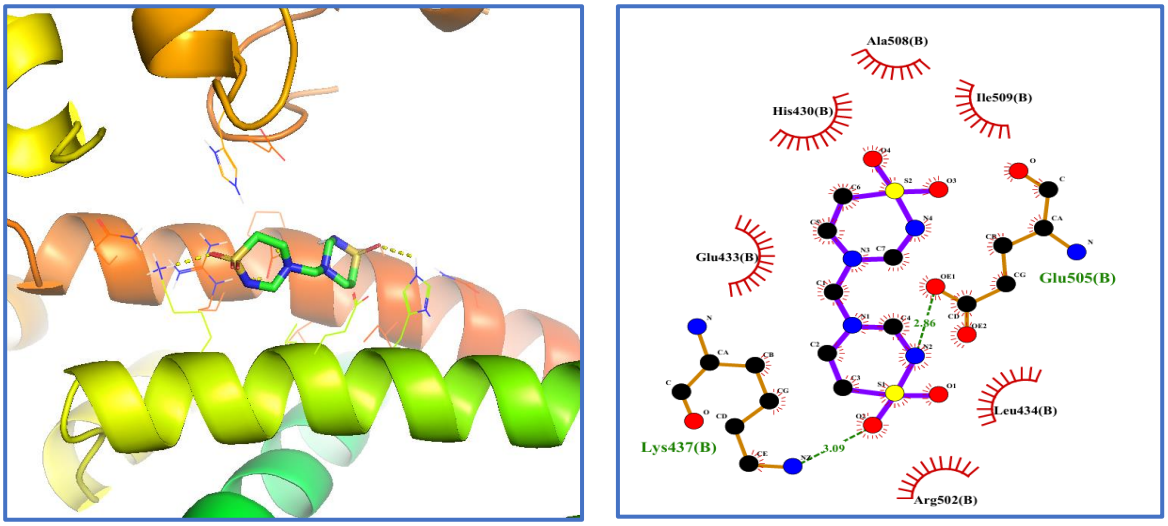

Figure 9b. Native structure of protein

Table 5. Second-order perturbation theory of fock matrix in selected NBO basis for taurolidine

Donor (i)	Type	Acceptor (j)	Type	Type of transition	E(2)[a] (KJ/mol)	E(j)-E(i)[b] (a.u)	F(i,j)[c] (a.u)
O3	LP(2)	S1-C16	σ*	LP(2)- σ*	17.54	0.41	0.076
O3	LP(3)	S1-O4	σ*	LP(3)- σ*	17.35	0.58	0.091
O3	LP(3)	S1-N9	σ*	LP(3)- σ*	16.35	0.41	0.074
O4	LP(2)	S1-C16	σ*	LP(2)- σ*	18.48	0.41	0.078
O4	LP(3)	S1-O3	σ*	LP(3)- σ*	14.33	0.58	0.083
O4	LP(3)	S1-N5	σ*	LP(3)- σ*	15.88	0.41	0.082
O5	LP(2)	S3-C17	σ*	LP(2)- σ*	17.54	0.41	0.076
O5	LP(3)	S2-O6	σ*	LP(3)- σ*	17.34	0.58	0.091
O5	LP(3)	S2-N10	σ*	LP(3)- σ*	16.36	0.41	0.074
O6	LP(2)	S2-C17	σ*	LP(2)- σ*	18.48	0.41	0.078
O6	LP(3)	S2-O5	σ*	LP(3)- σ*	14.33	0.58	0.083
O6	LP(3)	S2-N10	σ*	LP(3)- σ*	19.88	0.41	0.082

Table 6. Mulliken charges distribution of taurolidine

S. No.	Atoms	Charges	S. No.	Atoms	Charges
1	S_1	0.4379	18	H_{18}	0.154993
2	S_2	0.437884	19	H_{19}	0.154995
3	O_3	-0.22785	20	H_{20}	0.196268
4	O_4	-0.11353	21	H_{21}	0.192723
5	O_5	-0.22785	22	H_{22}	0.196268
6	O_6	-0.11353	23	H_{23}	0.192723
7	N_7	0.235882	24	H_{24}	0.234855
8	N_8	0.235866	25	H_{25}	0.173474
9	N_9	-0.28325	26	H_{26}	0.234853
10	N_{10}	-0.28323	27	H_{27}	0.173474
11	C_{11}	-0.65609	28	H_{28}	0.245238
12	C_{12}	-0.2208	29	H_{29}	0.239553
13	C_{13}	-0.22079	30	H_{30}	0.245237
14	C_{14}	-0.46957	31	H_{31}	0.239555
15	C_{15}	-0.46958	32	H_{32}	0.313581
16	C_{16}	-0.78142	33	H_{33}	0.313577
17	C_{17}	-0.78141	-	-	-

Table 7. Molecular docking of Taurolidine against 3TX7 protein

Ligand	Taurolidine
PDB ID	3TX7
Binding energy (Kcal/mol)	-6.86
No. of hydrogen bonding	2
Amino acids	Glutamic acid 505, Lysine 437
Bond length (Å)	2.86, 3.09
Hydrophobic interaction	Histidine 430 Glutamic acid 433 Arginine 505 Leucine 434 Isoleucine 509 Alanine 508

pathogenesis, including cancers, making it a critical therapeutic target for drug development. In the present study, it can be concluded that taurolidine exhibits favorable pharmacological properties and acts as a potent beta-catenin inhibitor. These findings will be helpful for researchers in future experimental (in vivo and in vitro) research on taurolidine.

4. Conclusion

The quantum chemical computational method (DFT) was utilized to explore structural, spectroscopic, and electronic characterization of taurolidine. The spectroscopic wavenumbers confirm the presence of SO_2, CH_2, NH, and CN functional groups. The bands simulated at 1076 and 1072 cm-1 with a PED contribution of 70 and 69% confirm SO_2 groups. In the electronic spectrum, a strong peak was observed at 203 (gas), 202 (ethanol and water), and 201 (chloroform and toluene) by H → L transitions. Compared with polar solvents, the energy gap of nonpolar solvents has increased, confirming their stability and reactivity in polar solvents. In NBO, the stabilization of interaction between electron-donating lone pair oxygen O6 to antibonding S2-N10 with the stabilizing energy of 19.88 KJ/mol by the transition of LP(3)- σ* contributes to the maximum stabilization. In Mulliken charge distribution, the carbon atoms C17 (-0.78141e) and C16 (-0.78142e) have increased negative potential as a result of the sulfonyl (SO_2) group in the ortho positions, and the outputs were closely confirmed by MEP analysis. In ELF and LOL, the hydrogens H24 (salvaged between nitrogen atoms) and H31 (linked with the sulfonyl group) are masked with red regions, deciphering the localized regions of electrons. The molecular docking prediction affirms that taurolidine exhibits significant antagonist properties against β-catenin protein with a binding affinity of -6.86 KJ/mol by forming two and six polar and nonpolar interactions, respectively.

References

[1] F.W. Guo, Q. Zhang, Y.C. Gu, C.L. Shao, Sulfur-containing marine natural products as leads for drug discovery and development, Current Opinion in Chemical Biology, 75 (2023) 102330, https://doi.org/10.1016/j.cbpa.2023.102330

[2] M. Mustafa, J.Y. Winum, The importance of sulfur-containing motifs in drug design and discovery, Expert opinion on drug discovery, 17(5) (2022) 501-512, https://doi.org/10.1080/17460441.2022.2044783

[3] D. Dordevic, J. Capikova, S. Dordevic, B. Tremlova, M. Gajdacs, I. Kushkevych, Sulfur content in foods and beverages and its role in human and animal metabolism: A scoping review of recent studies, Heliyon, 9(4) (2023) e15452, https://doi.org/10.1016/j.heliyon.2023.e15452

[4] M.L. Shankaranarayana, B. Raghavan, K.O. Abraham, C.P. Natarajan, H.H. Brodnitz, Volatile sulfur compounds in food flavors, CRC Crit. Rev. Food Technol, 4 (1974) 395-435, https://doi.org/10.1080/10408397409527163

[5] K. Sugio, D. Inoda, M. Masuda, I. Azumaya, S. Sasaki, K. Shimono, V. Ganapathy, S. Miyauchi, Transport of 2,4-dichloro phenoxyacetic acid by human Na+- coupled monocarboxylate transporter 1 (hSMCT1, SLC5A8), Drug Metabol. Pharmacokinet. 34 (2019) 95–103, https://doi.org/10.1016/j.dmpk.2018.10.004

[6] E. Rampler, T. Dalik, G. Stingeder, S. Hann, G. Koellensperger, Sulfur containing amino acids – challenge of accurate quantification, J. Anal. At. Spectrom. 27 (2012) 1018, https://doi.org/10.1039/c2ja10377j

[7] P. M. Neary, P. Hallihan, J. H. Wang, R. W. Pfirrmann, D. J. Bouchier-Hayes, H. P. Redmond, The evolving role of taurolidine in cancer therapy, Ann Surg Oncol, 17 (2010) 1135-1143, https://doi.org/10.1245/s10434-009-0867-9

[8] Y.T. Wang, P.C. Yang, Y.F. Zhang, J.F. Sun, Synthesis and clinical application of new drugs approved by FDA in 2023. European Journal of Medicinal Chemistry, 265 (2024)116124, https://doi.org/10.1016/j.ejmech.2024.116124

[9] M. McCourt, J.H. Wang, S. Sookhai, H. P Redmond, Taurolidine inhibits tumor cell growth in vitro and in vivo, Ann Surg Oncol, 7 (2000) 685-691, https://doi.org/10.1007/s10434-000-0685-6

[10] A. Mikolajczyk, V. Khosrawipour, H. Lau, S. Li, P. Migdal, M.K. Labbe, W. Kielan, J. Nicpon, S. Stieglitz, T. Khosrawipour, Exploring the potential of taurolidine in inducing mobilization and detachment of colon cancer cells: a preliminary in-vitro study. BMC Pharmacology and Toxicology, 23(1) (2022) 38, https://doi.org/10.1186/s40360-022-00572-8

[11] C. Lv, Y. Li, T. Wang, Q. Zhang, J. Qi, M. Sima, E. Li, T. Qin, Z. Shi, F. Li, X. Wang, Taurolidine improved protection against highly pathogenetic avian influenza H5N1 virus lethal-infection in mouse model by regulating the NF-κB signaling pathway. Virologica Sinica, 38(1) (2023)119-127, https://doi.org/10.1016/j.virs.2022.11.010

[12] I. Bedrosian, R. Duane Sofia, S.M. Wolff, C.A. Dinarello, Taurolidine, an analogue of the amino acid taurine, suppresses interleukin-1 and tumor necrosis factor synthesis in human peripheral blood mononuclear cells, Cytokine, 3(6) 1991 568-575, https://doi.org/10.1016/1043-4666(91)90483-T

[13] S. Vennila, K. Deepa, K.S. Nagaraja, L. Lakshmi, S. Selvaraj, C. Karnan, Synthesis, structural, spectral, Anticancer activity, and density functional theory investigations of 2-[hydrazinylidene (phenyl) methyl] pyridine. Journal of Molecular Structure, 1316 (2024) 138832, https://doi.org/10.1016/j.molstruc.2024.138832

[14] A. Ram Kumar, C. Senthamil Selvi, S. Selvaraj, G.P. Sheeja Mol, P. Jayaprakash, In silico studies on the molecular geometry, FMO, mulliken charges, MESP, ADME and molecular docking prediction of pyrogallol carboxaldehydes as potential anti-tumour agents, Phys. Chem. Res. 12 (2) (2024) 305–320, https://doi.org/10.22036/PCR.2023.402835.2359

[15] S. Selvaraj, P. Rajkumar, M. Kesavan, K. Thirunavukkarasu, S. Gunasekaran, N.S. Devi, S. Kumaresan, Spectroscopic and structural investigations on modafinil by FT-IR, FT-Raman, NMR, UV–Vis and DFT methods. Spectrochim. Acta A. 224 (2020) 117449, https://doi.org/10.1016/j.saa.2019.117449

[16] I.M. Chandramalar, V.P. Subhasini, Vibrational spectroscopic analysis of 2, 3: 4, 5-Bis-O-(1-methylethylidene) beta-D-fructopyranose Sulfamate (Topiramate) by density functional method. Spectrochimica Acta Part A: Molecular and Biomolecular Spectroscopy, 302 (2023) 122997, https://doi.org/10.1016/j.saa.2023.122997

[17] K. Vibha, N.C. Prachalith, R.A. Reddy, M.N. Ravikantha, J. Thipperudrappa, Computational studies on sulfonamide drug molecules by density functional theory, Chemical Physics Impact, 6 (2023) 100147, https://doi.org/10.1016/j.chphi.2022.100147

[18] M.J. Frisch, et al., Gaussian 09, Gaussian, Inc., Wallingford CT, (2009).

[19] W. Kohn, L.J. Sham, Self-consistent equations including exchange and correlation effects, Phy. Rev. 140 (1965) A1133-A1138, https://doi.org/10.1103/PhysRev.140.A1133

[20] A.D. Becke, Density functional thermo chemistry – I: The effect of the exchange only gradient

correlation, J. Chem. Phy. 98 (1993) 5648-5652, https://doi.org/10.1063/1.462066

[21] C. Lee, W. Yang, and R.G. Parr, Development of the Colle-Salvetti correlation-energy formula into a functional of the electron density, Phy. Rev. B. 37 (1988) 785-789, https://doi.org/10.1103/PhysRevB.37.785

[22] W.J. Hehre, R. Ditchfield, and J.A. Pople, Self-Consistent Molecular Orbital Meth- ods. XII. Further Extensions of Gaussian-Type Basis Sets for Use in Molecular Orbital Studies of Organic Molecules. The Journal of Chemical Physics 56(5), (1972): 2257–2261. https://doi.org/10.1063/1.1677527

[23] J.R. Cheeseman, G.W. Trucks, T.A. Keith, and M.J. Frisch, A comparison of models for calculating nuclear magnetic resonance shielding tensors. The Journal of Chemical Physics 104, (1996) 5497–5509.

[24] M. Petersilka, U.J. Gossman, E.K.U. Gross, Excitation energies from time-dependent density-functional theory, Phy. Rev. Lett. 76 (1966) 1212-1215, https://doi.org/10.1103/PhysRevLett.76.1212

[25] E. Runge, E.K.U. Gross, Density functional theory for time-dependent systems, Phy. Rev. Lett. 52 (1984) 997, https://doi.org/10.1103/PhysRevLett.52.997

[26] N. M. O'Boyle, A. L. Tenderholt and K. M. Langner. J. Comp. Chem., 2008, 29, 839-845.

[27] R. Dennington, T.A. Keith, J.M. Millam GaussView 6.0. Semichem Inc., Shawnee Mission, KS, USA (2016)

[28] G.A. Zhurko, D.A. Zhurko, Chemcraft Program Version 1.6 (Build 315), 2009, http://www.chemcraftprog.com

[29] T. Lu, F. Chen, Multiwfn: a multifunctional wavefunction analyzer, J. Comput. Chem. 33 2012 580-592, https://doi.org/10.1002/jcc.22885

[30] G.M. Morris, R. Huey, W. Lindstrom, M.F. Sanner, R.K. Belew, D.S. Goodsell, A.J. Olson, AutoDock4 and AutoDockTools4: Automated docking with selective receptor flexibility, J. Comput. Chem. 30 (2009: 2785-2791, https://doi.org/10.1002/jcc.21256

[31] W.L. DeLano, Pymol: an open-source molecular graphics tool. CCP4 News letter on protein Crystallography, 40(1) (2002) 82–92.

[32] A.C. Wallace, R.A. Laskowski, J.M. Thornton, LIGPLOT: a program to generate schematic diagrams of protein–ligand interactions, Protein. Eng. Des. Sel. 8 (1995) 127-134, https://doi.org/10.1093/protein/8.2.127

[33] F. Caruso, J. W. Darnowski, C. Opazo, A. Goldberg, N. Kishore, E.S. Agoston, M. Rossi, Taurolidine Antiadhesive Properties on Interaction with E.coli; Its Transformation in Biological Environment and Interaction with Bacteria Cell Wall, (2010), https://doi.org/10.1371/journal.pone.0008927

[34] X. Liu, T. Liao, N. Yang, S. Ban, Y. Wang, Z. Zheng, Z. Zhou, Synthesis, crystal and molecular structures, DFT calculations, spectroscopic (IR, NMR, UV–Vis), vibrational properties and Hirshfeld surface and antitumor activity of two pyrazole boronic acid pinacol ester compounds. Journal of Molecular Structure, 1299 (2024) 137204, https://doi.org/10.1016/j.molstruc.2023.137204

[35] S. Selvaraj, A. Ram Kumar, T. Ahilan, M. Kesavan, S. Gunasekaran, S. Kumaresan, Multi spectroscopic and computational investigations on the electronic structure of oxyclozanide, J. Indian. Chem. Soc. 99(10) (2022) 100676, https://doi.org/10.1016/j.jics.2022.100676

[36] A. Ram Kumar, S. Selvaraj, N. Kanagathara, Spectroscopic, Structural and Molecular Docking Studies on N, N-Dimethyl-2-[6-methyl-2-(4-methylphenyl) Imidazo [1, 2-a] pyridin-3-yl] Acetamide, Phys. Chem. Res.12(1) (2024) 95-107, https://doi.org/10.22036/PCR.2023.387911.2306

[37] C. Karnan, A. Ram Kumar, S. Selvaraj, Quantum Chemical Computational Studies on the Structural Aspects, Spectroscopic Properties, Hirshfeld Surfaces, Donor-Acceptor Interactions and Molecular Docking of Clascosterone: A Promising Antitumor Agent. International Research Journal of Multidisciplinary Technovation, 6(4) (2024) https://doi.org/10.54392/irjmt2444

[38] A. Ram Kumar, S. Selvaraj, M. Azam, G.P. Sheeja Mol, N. Kanagathara, M. Alam, P. Jayaprakash, Spectroscopic, biological, and topological insights on lemonol as a potential anticancer agent, ACS Omega, 8(34) (2023) 31548–31566, https://doi.org/10.1021/acsomega.3c04922

[39] A. Ram Kumar, S. Selvaraj, G. Sheeja Mol, M. Selvaraj, L. Ilavarasan, S.K. Pandey, P. Jayaprakash, S. Awasthi, O. Albormani, A. Ravi, Synthesis, solvent-solute interactions (polar and nonpolar), spectroscopic insights, topological aspects, Fukui functions, molecular docking, ADME, and donor-acceptor investigations of 2-(trifluoromethyl) benzimidazole: A promising candidate for antitumor pharmacotherapy, J. Mol. Liq. 393 (2023) 123661, https://doi.org/10.1016/j.molliq.2023.123661

[40] W. Gong, P. Li, S. Rohani, Taurine in several aqueous binary solvents: solubility prediction, measurement, modeling, solvent effect, and thermodynamics. Journal of Molecular Liquids, 367 (2022) 120522, https://doi.org/10.1016/j.molliq.2022.120522

[41] P. Divya, V.J. Reeda, S. Selvaraj, B. Jothy,

Theoretical spectroscopic electronic elucidation with polar and non-polar solvents (IEFPCM model), molecular docking and molecular dynamic studies on bendiocarb-antiallergic drug agent. Journal of Molecular Liquids, 404 (2024) 124895, https://doi.org/10.1016/j.molliq.2024.124895

[42] S. Selvaraj, Computational study on the structural features, vibrational aspects, chemical shifts, and electronic properties of 1,4- Dinitrosopiperazine-2-carboxylic acid: Insights into donor-acceptor interactions and thermodynamic properties, International Research Journal of Multidisciplinary Technovation, 6(1), 2024, 1-16, https://doi.org/10.54392/irjmt2411

[43] G. P, Sheeja Mol, D. Aruldhas, I. Hubert Joe, S. Selvaraj, G. Anuroopa, A. Nadh, J. Kunhikrishnan, Quantum chemical investigations, Hirschfeld surface analysis, FMO, MESP, topology analyses, in-silico analysis and pharmacokinetics properties of 3-chloro-N-(4-hydroxy-3-methoxy-benzyl)-2, 2-dimethyl propanamide [CHMBDP]. Molecular Crystals and Liquid Crystals, (2024) 1-17, https://doi.org/10.1080/15421406.2024.2381292

[44] P. Jayaprakash, S. Selvaraj, A. Ram Kumar, A new organic compound (C9H12N2O2): crystal structure, characterization, Hirshfeld surface analysis, electronic properties, NLO properties, DFT calculation and molecular docking. Solid State Sciences, (2024) 107587, https://doi.org/10.1016/j.solidstatesciences.2024.107587

[45] P. Divya, V.J. Reeda, S. Renuga, C.D. Annapoorani, V.B. Jothy, Vibrational analysis, DFT computations of spectroscopic, non-covalent analysis with molecular docking and dynamic simulation of 2-amino-4, 6-dimethyl pyrimidine benzoic acid. Journal of Molecular Structure, 1318 (2024) 139160, https://doi.org/10.1016/j.molstruc.2024.139160

Authors Contribution Statement

Both the authors equally contributed to this work. Also, read and approved the final version of the manuscript

Funding

The authors declare that no funds, grants or any other support were received during the preparation of this manuscript.

Competing Interests

The authors declare that there are no conflicts of interest regarding the publication of this manuscript.

Has this article screened for similarity?

Yes

Data Availability

The data supporting the findings of this study can be obtained from the corresponding author upon reasonable request.

About the License